American Mineralogist, Volume 101, pages 2731–2737, 2016

Transformation of pyrite to pyrrhotite in the presence of Au-Ag alloys at 500 °C

Galina Palyanova[1,2,*], Konstantin Kokh[1,2], and Yurii Seryotkin[1,2]

[1]Sobolev Institute of Geology and Mineralogy, Siberian Branch of the RAS, Koptyuga ave., 3, Novosibirsk 630090, Russia
[2]Novosibirsk State University, Pirogova str., 2, Novosibirsk 630090, Russia

Abstract

Dry annealing of Au_xAg_{1-x} alloys (x = 0.19, 0.35, 0.56 or of fineness 300, 500, 700‰) and pyrite was used to reveal the solubility of Au (Ag) in FeS_2 and study phase equilibria in the FeS_2-Au_xAg_{1-x} system at 500 °C. Pyrrhotite, acanthite, and uytenbogaardtite and Au-Ag alloys with increased fineness were established at the contacts of pyrite blocks with Au-Ag plates. The obtained results evidence the absence of solubility between FeS_2 and Au (Ag) at 500 °C. The Ag content in alloys influences the stability of pyrite and contributes to its transformation in pyrrhotite and sulfidation and ennobling of Au-Ag alloys. Au-Ag sulfides and pyrrhotite may be present in the sulfide ores of metamorphogene deposits as annealing products of Au-Ag-pyrite-bearing ores.

Keywords: Desulfidation, pyrite, pyrrhotite, visible and "invisible" gold (silver), isomorphism, thermodiffusion, sulfidation, ennobling of Au-Ag alloys, Au-Ag sulfides

Introduction

Pyrite is the most well-known and widespread mineral of the iron sulfides. It is a common constituent of many igneous, metamorphic, and sedimentary types of rocks and of hydrothermal veins. More important is the fact that pyrite is a collector of gold and silver (Boyle 1968, 1979). Revealing the forms of occurrence of noble metals in iron sulfides is of fundamental and applied importance. Pyrite often contains micro inclusions of native gold, Ag-Au chalcogenides and other minerals of gold and silver that are visible under optical microscope and scanning electron microscope (Zhou et al. 2004; Palyanova et al. 2015a, 2016). It has been established so far that "invisible" gold occurs as submicrometer or nano-sized inclusions or solid solution in the structure of iron sulfides (Vikentyev 2015 and its reference list). The amount of isomorphous gold incorporated into pyrite lattice covers a wide range of values as reported by some authors (Fleischer 1955; Cook and Chryssoulis 1990; Abraitis et al. 2004; Vaughan 2004; Pal'yanova et al. 2015b). Gold and silver concentrations in pyrites range from below one parts per million to almost thousand parts per million.

To determine the probability of incorporation of gold and silver into pyrite, we conducted experiments of solid-phase diffusion (Jin 1981), using natural pure pyrite and synthetic Au-Ag alloys of varying composition. According to this technique, if the plates of two substances A and B are brought into contact and then kept at temperature when diffusion is probable, their composition finally becomes homogeneous. If isomorphism between two components is absent, various compounds stable in the A-B system are formed in the contact zone. This technique is successfully applied to study many binary and ternary systems and construction of the isothermal sections of phase diagrams (Kodentsov et al. 2001). However, this technique has restrictions; melting should be avoided. Data from the phase diagram Fe-S (Kullerud and Yoder 1959; Arnold 1962; Waldner and Pelton 2005; Wang and Salveson 2005) evidence that pyrite is unstable at temperatures above 742–745 °C and melts incongruently with formation of pyrrhotite and sulfur. At temperatures between the melting point and 325 °C, pyrite coexists with pyrrhotite of various compositions $Fe_{1-y}S$ ($0.78 < y < 1$) or FeS_x ($1 < x < 1.23$). To avoid melting of pyrite, the specified temperature in the experiments was 500 °C. Application of this technique allows studying phase equilibria in the FeS_2-Au_xAg_{1-x} system. One of the tasks of the investigation was to study the behavior of noble metals in the process of desulfidation of pyrite (Craig and Vokes 1993; Thomas et al. 2011) and sulfidation of native gold (Pal'yanova et al. 2014), which are typical of natural processes.

Experiments and analytical methods

Starting compositions

In the experiments we used a large natural pyrite single crystal from the Berezovskoe gold-quartz deposit (Ural, Russia). Microprobe analysis showed that pyrite crystal is homogeneous and does not contain micro impurities. First, a plate ~5–6 mm thick was cut from the crystal. After polishing on 1 μm diamond paste, the plate was cut into bars with polished area ~3 × 3 mm. Gold-silver alloys of $Au_{0.19}Ag_{0.81}$, $Au_{0.35}Ag_{0.65}$, and $Au_{0.56}Ag_{0.44}$ composition [gold fineness = 1000×Au/(Au+Ag), by weight, 300, 500, and 700‰, respectively] synthesized from a stoichiometric mixture of pure metals were rolled out to the thickness of ~200 μm and cut into plates measuring 3 × 3 mm. Then metal sheets were placed between polished surfaces of the pyrite bars, and the resulting column was sealed under 10^{-3} torr in the quartz ampoule. The samples were slowly heated to 500 °C in the isothermal zone of the furnace and kept at this temperature for 7 days. After annealing, the ampoule was cooled to room temperature in the switched off furnace.

Analytical techniques

Optical microscopy, scanning electron microscopy (SEM), electron microprobe analysis (EPMA), and X-ray powder diffraction methods were applied to study the samples. A polished section was prepared from the synthesized phases for microscopy analyses. Studies on the chemical composition of the synthesized substances were carried out using MIRA 3 LMU SEM (TESCAN Ltd.) combined with the microanalysis systems INCA Energy 450+ on the basis of the high-sensitivity silicon

* E-mail: palyan@igm.nsc.ru

0003-004X/16/0012–2731$05.00/DOI: http://dx.doi.org/10.2138/am-2016-5808

drift detector XMax-80 and INCA Wave 500 (Oxford Instruments Nanoanalysis Ltd.) (Analytical Center for Multielemental and Isotope Research SB RAS (Russia, Novosibirsk, analyst N.S. Karmanov). The analyses were conducted at 20 kV accelerating voltage, 1.5 nA probe current. Most analyses of Au-Ag sulfides were performed using SEM-EDS at 15–20 s live acquisition time of spectrum. Acquisition of spectra was performed in the raster mode with the scanning area from 0.5 × 0.5 μm² for fine phases, and to 2 × 2 μm² for larger phases with a slightly defocused electron beam. While a bulk composition of decay structures was obtained with the scanning area from 5 × 5 to 10 × 10 μm². The analyses were made with a slightly defocused electron beam, to reduce the destructive effects of the electron beam on unstable Au-Ag sulfides. For analysis we used the characteristic X-ray S *K*-series and *L*-series of Ag and Au. Under these conditions the random error of measurement caused by the counting statistic for Au-Ag sulfide, corresponding to uytenbogaardtite was 0.17, 0.37, and 0.98 wt% for S, Ag, and Au, respectively. Detailed measurement techniques have been worked out for the natural Au-Ag sulfides and described in (Palyanova et al. 2014). Pure silver and gold, PbS and $CuFeS_2$, were used as standards for Ag, Au, S, and Fe, respectively.

X-ray powder diffraction study of the synthesized phases was performed on a Stoe IPDS-2T diffractometer (Mo*Kα* radiation, graphite monochromator) using Gandolfi mode. Two-dimensional X-ray patterns were radially integrated using the XArea software package. The diffraction profiles were treated by using the WinXPow (Stoe) program packages. For the phase analysis, the database of PDF-4 Minerals (The Powder Diffraction File PDF-4 +, 2006) was used.

Results

The data on solid phase products of experiments are given in Table 1. The reaction zones between pyrite blocks and Au-Ag alloys contained pyrrhotite, acanthite-, and uytenbogaardtite phases and Au-Ag alloys of fineness higher than the initial fineness, but lower than 830‰ (Figs. 1 and 2). It was established that pyrrhotite in all three zones had an identical and stable composition very close to Fe_7S_8. Analysis of Au-Ag alloys shows up to 1.6 wt% of sulfur, which may be explained by micro inclusions of Au-Ag sulfides. The fineness of alloys was calculated without account of sulfur. Acanthite and uytenbogaardtite form the structures of solid-solution decay. SEM photos made at high magnification (Figs. 3a–3c) show two phases of Au-Ag sulfides well discriminated by color: acanthite (gray) and uytenbogaardtite (light gray). It is supposed that this aggregate reflects the possible composition of the Au-A sulfide solid solution stable at 500 °C (Table 1).

The amount of acanthite phase prevails in all experiments. According to EPM analysis, the mole ratios of metals to sulfur (Ag+Au)/S in the acanthite and uytenbogaardtite phases vary from 1.5 to 1.6, which is considerably lower compared to their ideal compositions. This may be described by the visually observed partial decomposition of the phases under ion beam. The features of phases and chemical compositions of each reaction zone are described below:

Pyrite + Ag-Au alloy (300‰). In the reaction zone with initial low-fineness alloy we established alloys with the fineness

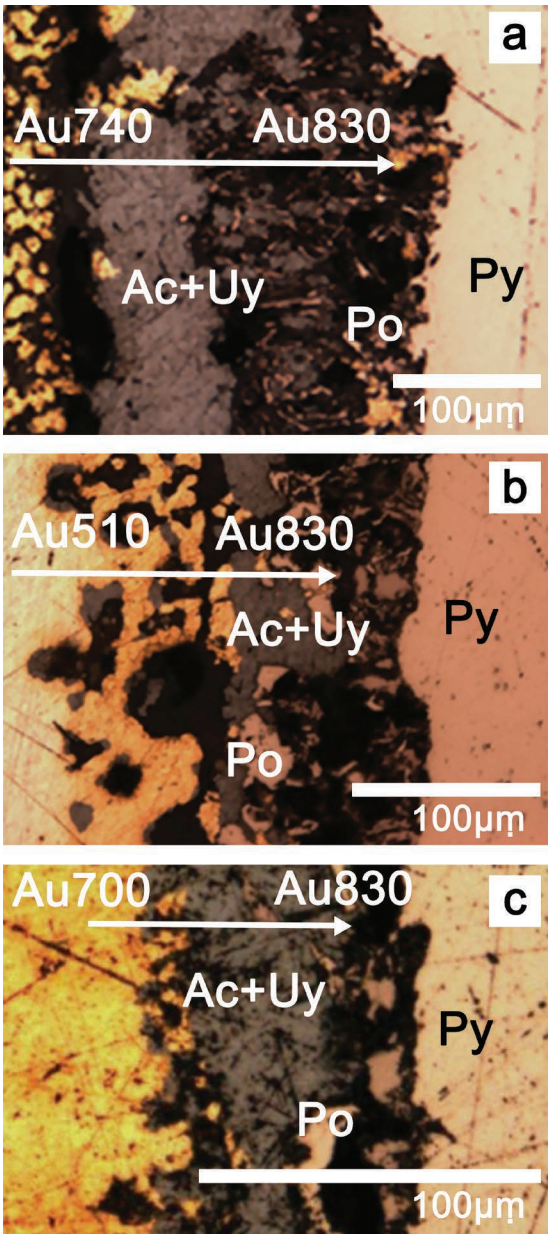

Figure 1. Photo (in reflected light) of polished sections: phases in the reaction zone formed at the contact of pyrite and Au-Ag alloys of fineness 300‰ (**a**), 500‰ (**b**), and 700‰ (**c**). Symbols of the phases: Py = pyrite, Po = pyrrhotite, Ac = acanthite, Uy = uytenbogaardtite, N_{Au} = fineness of Au-Ag alloys (‰). (Color online.)

Table 1. Initial fineness (N_{Au}) and compositions of Au-Ag alloys and compositions of new phases formed at the contact Au-Ag alloys and pyrite at 500 °C

No.	Initial Au-Ag alloys (N_{Au} ‰)	Compositions of new phases				
		Au-Ag alloys (N_{Au} ‰)	Au-Ag sulfides 25 °C	Au-Ag sulfide ss 500 °C[a]	Au-Ag sulfide ss (reaction 2)[b]	Iron sulfide
1	$Au_{0.19}Ag_{0.8}$[a] (300)	$Au_{0.61}Ag_{0.39}$ (740)	Ac ($Ag_{>1.54-1.61}S$)	$Ag_{1.60}Au_{0.26}S$	$Ag_{1.69}Au_{0.31}S$	$Fe_{0.875}S$
		$Au_{0.72}Ag_{0.28}$ (830)	Uy ($Ag_{2.98}Au_{0.84}S_2$)	$Ag_{1.71}Au_{0.29}S$		
2	$Au_{0.35}Ag_{0.65}$ (500)	$Au_{0.36}Ag_{0.64}$ (510)	Ac ($Ag_{1.60}Au_{0.05}S$)	$Ag_{1.62}Au_{0.06}S$	$Ag_{1.30}Au_{0.70}S$	$Fe_{0.875}S$
		$Au_{0.73}Ag_{0.27}$ (830)	Uy ($Ag_{3.26}Au_{0.50}S_2$)	$Ag_{1.36}Au_{0.64}S$		
3	$Au_{0.56}Ag_{0.44}$ (700)	$Au_{0.56}Ag_{0.44}$ (700)	Ac ($Ag_{1.50}Au_{0.01}S$)	$Ag_{1.55}Au_{0.03}S$	$Ag_{1.28}Au_{0.72}S$	$Fe_{0.875}S$
		$Au_{0.73}Ag_{0.27}$ (830)	Uy ($Ag_{3.12}Au_{0.17}S_2$)	$Ag_{1.28}Au_{0.72}S$		

[a] Compositions of acanthite-uytenbogaardtite mixture, obtained with the scanning extended area with a slightly defocused electron beam at EPMA.
[b] Calculated compositions of the solid sulfide solutions on reaction 2 for a = 13 and c = 1 according to the measured range of Au-Ag alloys in each sample (column 3 left).

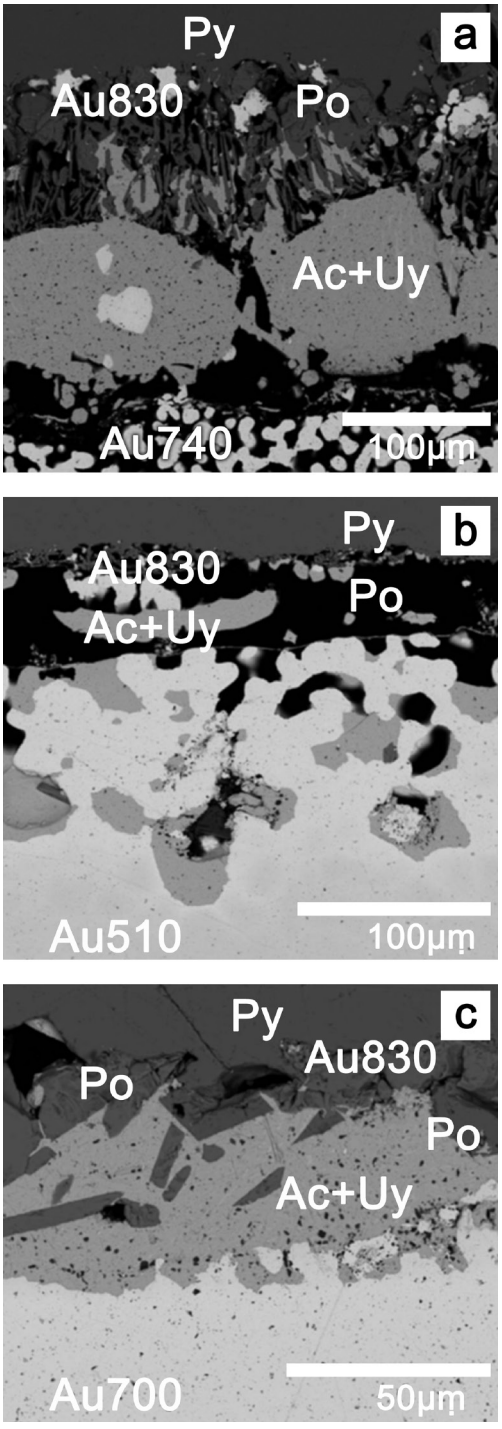

Figure 2. SEM photo of phases in the reaction zone formed at the contact of pyrite and Au-Ag alloys of fineness 300‰ (**a**), 500‰ (**b**), and 700‰ (**c**).

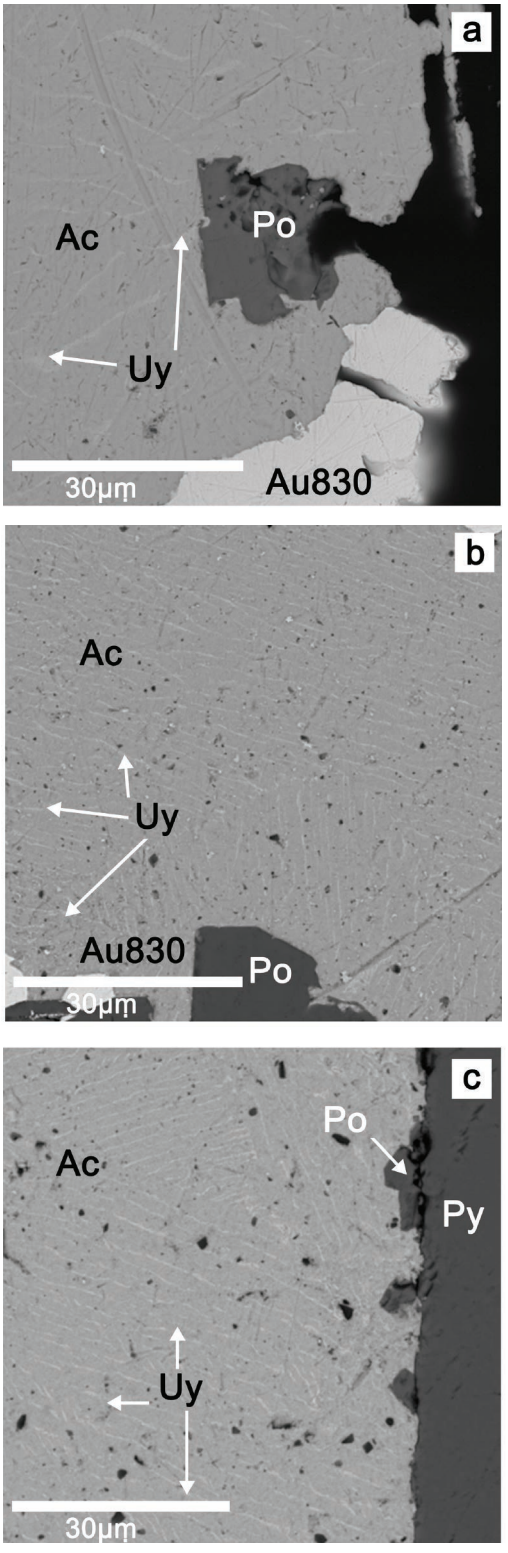

Figure 3. SEM photo of Au-Ag sulfides (acanthite and uytenbogaardtite phases) formed at the contact of pyrite and Au-Ag alloys of fineness 300‰ (**a**), 500‰ (**b**), and 700‰ (**c**) as well as their relationships and compositions.

from 830‰ near the pyrite to 740‰ in the middle part of the alloy plate (Figs. 1a and 2a; Table 1). Uytenbogaardtite forms parallel thin veinlets (less than 1–3 μm wide) in acanthite (Fig. 3a). The maximal content of gold reaches 29.4 wt% in uytenbogaardtite ($Ag_{2.98}Au_{0.84}S_2$). Acanthite was analyzed as

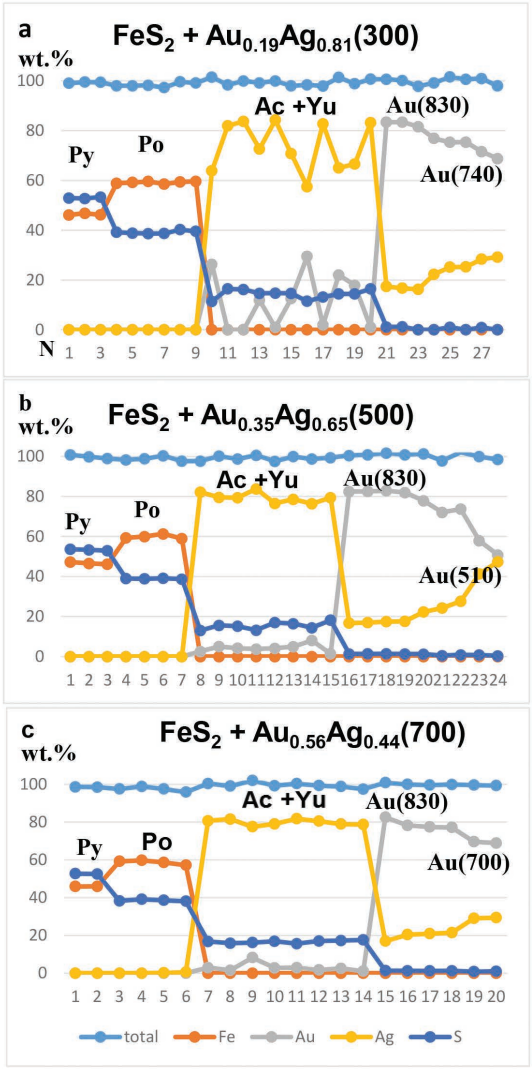

FIGURE 4. Cross section showing the content of elements (in wt%) and phases along the "reaction zones" between pyrite and Au-Ag alloys of fineness 300‰ (**a**), 500‰ (**b**), and 700‰ (**c**). (Color online.)

$Ag_{>1.61–1.54}S$. The possible bulk composition of the Au-Ag sulfide solid solution existing at 500 °C corresponds to the formula $Ag_{1.60}Au_{0.26}S$ (Table 1).

Pyrite + Ag-Au alloy (500‰). In the reaction zone with the initial alloy of medium fineness we have established alloys of fineness from 520 to 830‰ (Figs. 1b and 2b; Table 1). In contrast to previous sample, the fineness of alloy has varied more slightly remaining almost unchanged in the center (Fig. 4b). Gold content does not exceed 8 wt% in Au-Ag sulfides. Au-Ag sulfides are presented by two phases (Fig. 3b): acanthite ($Ag_{1.60}Au_{0.05}S$) and uytenbogaardtite ($Ag_{3.26}Au_{0.50}S$). The possible composition of Au-Ag sulfide solid solution stable at 500 °C is equal to $Ag_{1.62}Au_{0.06}S$ (Table 1).

Pyrite + Ag-Au alloy (700‰). The alloy of a high fineness appeared to be most stable. The reaction zone in this experiment (Figs. 1c and 2c) is narrower than those with alloys of fineness 300‰ (Figs. 1a and 2a) and 500‰ (Figs. 1b and 2b). Purely unreacted areas of the alloy were found in the central parts. The maximum fineness of the reacted alloy, again, does not exceed 830‰. The fineness of alloys insignificantly increased from the center of the Au-Ag plate toward the contact with pyrite (Figs. 1c and 2c). In Au-Ag sulfides, gold concentration varies from 1.1 to 8.2 wt%. Two phases of Au-Ag sulfides were found: acanthite ($Ag_{1.50}Au_{0.01}S$) and uytenbogaardtite ($Ag_{3.12}Au_{0.17}S_2$). The possible bulk composition of the Au-Ag sulfide stable at 500 °C is equal to $Ag_{1.55}Au_{0.03}S$ (Table 1).

Figure 4 shows the variations of Fe, S, Au, and Ag concentrations along the reaction zones and new phases found between pyrite and Au-Ag alloys in each experiment. The same pattern of variations in Fe and S concentrations was established in all samples. The concentration of sulfur decreases in transition from pyrite to pyrrhotite and further to Au-Ag sulfides. Finally, its content becomes almost zero in Au-Ag alloys. Iron has the same behavior; its concentration falls to zero in Au-Ag alloys and Au-Ag sulfides. The alloy plates have considerable variation of Au/Ag ratio and the most constant composition was found in the sample with initial 300‰ fineness. A similar pattern of noble metals redistribution was found in each experiment (Figs. 4a–4c). Au content close to the contact with pyrite is maximal and appears to be higher than that in the initial alloy. While silver concentration is lower than in initial alloy and it gradually increases toward the center of alloy plate.

The estimations of the composition of sulfide solid solution at 500 °C showed that the maximum content of Au belongs to the sample with 300‰ plate. Impurities of noble metals were not found in pyrite and pyrrhotite or their content was lower than the detection limit of EPMA.

Figure 5 demonstrates redistribution of elements throughout the reaction zone formed at the contact of the 500‰ fineness alloy and pyrite. Compared with gold (Fig. 5b), the silver (Fig. 5a) is more intensively transferred from Au-Ag alloys to react with sulfur, which appeared as a result of pyrite desulfidation. The final products of reaction at 500 °C are Au-Ag sulfide solid solution, which decomposes at room temperature, and pyrrhotite Fe_7S_8 substituting pyrite (Fig. 5c).

X-ray powder diffraction results show that pyrite, pyrrhotite, acanthite, uytenbogaardtite, and Au-Ag alloys are present in each reaction zone (Fig. 6). In all samples, the peaks intensities of uytenbogaardtite phase are considerably lower than those of acanthite phase, which is confirmed by EPMA analyses (Figs. 3a–3c).

DISCUSSION

Data from Lambert et al. (1998) provide evidence that thermal decomposition of pyrite in the temperature range of 347–700 °C in vacuum proceeds with the formation of pyrrhotite and a gas phase that mainly consists of S_2:

$$FeS_2 = FeS_x + 0.5(2 - x)S_2(g) \qquad 1 < x < 1.23. \qquad (1)$$

And pyrrhotite composition is determined by the equation: $x = 1.45 \times 10^{-4} \times T(K) + 1.0354$. The composition of pyrrhotite calculated by this equation is 1.147, which is in good agreement with the data of microprobe analysis of pyrrhotite from the reaction zones (Fe_7S_8~$FeS_{1.14}$).

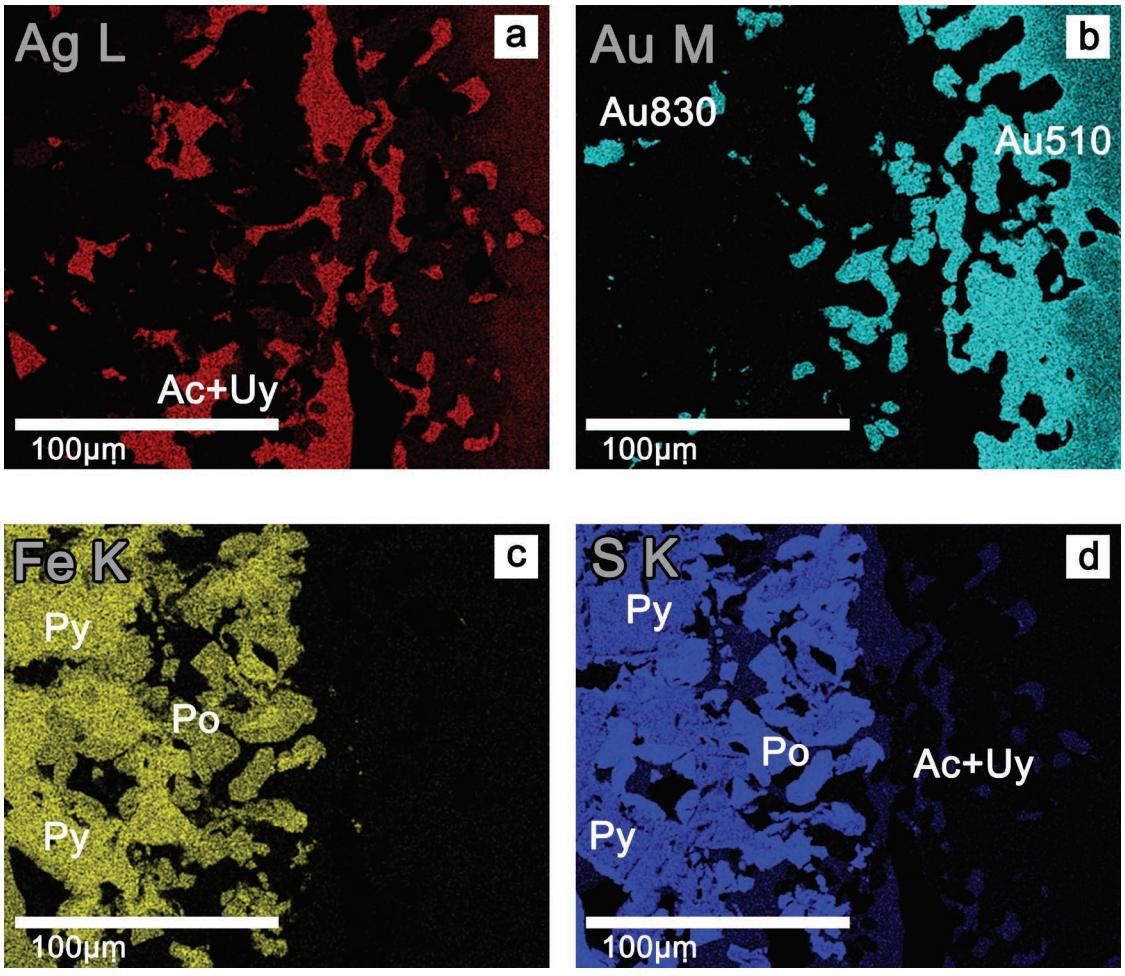

FIGURE 5. Distribution of elements Ag (**a**), Au (**b**), Fe (**c**), and S (**d**) in characteristic radiations (Ag$L\alpha_1$, Au$M\alpha_1$, Fe$K\alpha_1$, S$K\alpha_1$, respectively) over the scanning area of reaction zone formed at the contact of pyrite and alloy of fineness 500‰. (Color online.)

According to data of electrum-tarnish method (Barton and Toulmin 1964), at 500 °C in the presence of pyrite-pyrrhotite buffer the alloys of fineness lower 780‰ must be sulfidated and become black. In our experiments all three alloys have turned black due to sulfidations, which agrees with the previous data. In addition, we have found newly formed uytenbogaardtite and Au-enriched noble alloys. Francis (1971) investigated the kinetics and mechanism of electrum tarnish by sulfur. One of his results was a decrease of silver in Au-Ag alloys put in contact with silver sulfide.

Since pyrite blocks and Au-Ag plates were placed into one ampoule, the value of sulfur pressure was identical for all samples and was mainly determined by the pyrite-pyrrhotite buffer at 500 °C, and probably by some average activity of gold and silver in alloy plates.

Pyrite desulfidation is accompanied by a sulfidation reaction of Au-Ag alloys. According to the solid state products found in the reaction zones, the following quasi-reaction is assumed to take place between pyrite and Au-Ag alloys (in general mode):

$$7FeS_2 + aAu_xAg_{1-x} \rightarrow Fe_7S_8 + 6Ag_{2-y}Au_yS + cAu_zAg_{1-z}$$
$$(0 < x < 1,\ 0 < y < 1.1,\ x < z < 1,\ a > 12,\ c > 0). \quad (2)$$

The ternary $Ag_{2-y}Au_yS$ sulfides lie from Ag_2S to slightly beyond AgAuS (Barton 1980). From Equation 2 it is possible to estimate the compositions of Au-Ag sulfide solid solution. Table 1 contains the calculated variations in the solid solution according to the measured range of Au-Ag alloys in each sample. It may be concluded that the sample with 300‰ alloy is mostly close to the equilibrium since the EPMA data of Au-Ag sulfide solid-solution decay structures have shown the highest content of gold. Also, the fineness of resulting alloy has the shortest range 740–830‰ compared to 510–830 and 700–830‰ intervals found in the experiments with 500 and 700‰ initial alloys, respectively.

Au-Ag sulfide solid solution is unstable at room temperature and therefore it decomposes to form a mixture of acanthite and uytenbogaardtite or uytenbogaardtite and petrovskaite, according to Ag_2S–Au_2S phase diagram (Folmer et al. 1976; Barton 1980; Osadchii and Rappo 2004; Palyanova et al. 2011). When studying the system Fe-Au-S, it was impossible to synthesize Au_2S by a similar reaction with gold even at high temperatures and longer period of time (Barton and Toulmin 1964; Toulmin and Barton 1964). In the system Fe-Ag-Au-S, we obtained Ag-Au sulfides of various compositions through melt crystallization: Ag_2S, Ag_3AuS_2,

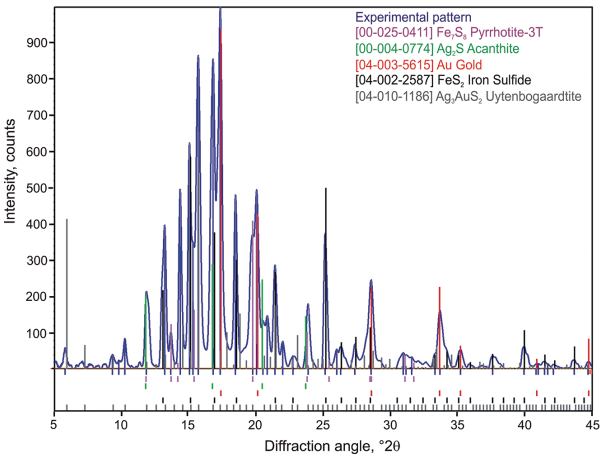

FIGURE 6. X-ray powder diffraction pattern of sample with 700‰ initial alloy. Vertical lines under graph represents the peaks position of (from top to bottom): Experimental pattern, gold, uytenbogaardtite Ag_3AuS_2, pyrite FeS_2, pyrrhotite Fe_7S_8, and acanthite Ag_2S. The bottom of the figure shows a bar chart for each phase in the same sequence as in the phase at the top of the list on the right. (Color online.)

AgAuS, and solid solutions $(Ag,Au)_2S$ together with pyrite and pyrrhotite (Palyanova et al. 2012). Ag sulfides were synthesized in the system Fe-Ag-S (Taylor 1970; Chareev and Osadchii 2006).

The sulfidation reactions of native gold with participation of S_2 gas were considered in a few papers (Barton et al. 1978; Barton 1980; Gurevich et al. 2011; Palyanova et al. 2014). These reactions may provide one or two phases of Au-Ag sulfides and ennobled alloys up to pure gold (Palyanova et al. 2014). The results of this work also evidence that sulfidation of Au-Ag alloys proceeds through a quasi-equilibria resulting in the formation of alloy with a higher fineness according to reaction 2.

The pyrite, close to or at a distance from the reaction zone, and the newly formed pyrrhotite contain no traces of gold and silver. It is worth noting that pyrite that was not at the contact with Au-Ag plates did not undergo any changes. These data suggest that gold and silver do not dissolve in pyrite and are not incorporated isomorphously into its structure.

It was established before that pyrite stability is controlled partly by temperature and pressure and partly by the amount of H_2O (Tomkins 2010). Our results suggest that in a dry system the presence of silver in the initial alloys seems to promote the reactions of desulfidation of pyrite and sulfidation of Ag-Au alloys. Interestingly the lower the fineness of initial alloys, the higher is the rate of desulfidation reaction of pyrite and parallel sulfidation reaction of Au-Ag alloys. In natural processes, pyrite containing micro-inclusions of native gold on heating will react with them to form pyrrhotite Fe_7S_8 and Au-Ag sulfides (acanthite, uytenbogaardtite, and petrovskaite) and higher fineness Au-Ag alloys. The presence of native gold inclusions, especially low fineness, in pyrite will promote pyrrhotite formation.

IMPLICATIONS

A great number of gold deposits are characterized by the presence of visible inclusions of native gold in pyrite and in the intergrain space of pyrite (Zhou et al. 2004). We predict the presence of Au-Ag sulfides with pyrrhotite for metamorphogene deposits with native silver, kustelite, electrum, and pyrite. Au-rich native gold is stable and less disposed to sulfidation in comparison to the Ag-rich alloys. Sulfidation reactions of native gold with the appearance of Au-Ag sulfides—acanthite, uytenbogaardtite, petrovskaite, or their mixtures (such as acanthite with uytenbogaardtite or uytenbogaardtite with petrovskaite)—are typical of some gold deposits (Palyanova et al. 2014, 2016). Au-Ag sulfides in association with pyrite and Fe-sphalerite were found in several mines: Konechnoe Au-quartz occurrence (Taimyr, Russia) (Proskurnin et al. 2011); Au-Ag deposits, Broken Hills adularia-sericite (Hauraki Goldfield, New Zealand) (Cocker et al. 2013); and Dzhulietta (northeastern Russia) (Palyanova et al. 2016). The number of deposits with uytenbogaardtite with petrovskaite is increasing every year (http://www.mindat.org/min-4127.html).

Along with a hypergeneous origin and crystallization from hydrothermal solutions, volcanic gases or sulfide melts (Cocker et al. 2013; Palyanova et al. 2011, 2012; Savva et al. 2012), these Au-Ag sulfides could be formed due to sulfidation of Au-Ag alloys in metamorphogene processes. According to the relationship between the fineness of alloy and the rate of pyrite/alloy reaction, the amount of resulting acanthite should prevail that of uytenbogaardtite and petrovskaite.

In the annealing products of Au-Ag-pyrite-bearing ores the presence of Au-Ag sulfides and pyrrhotite is also probable. The higher mobility of silver compared to gold during thermodiffusion at the contact of Au-Ag alloys with pyrite is one of the probable mechanisms of the increase in gold fineness and genesis of Au-Ag sulfides in nature. The presence of fine-grained micro inclusions of Au-Ag sulfides, which are hard to diagnose in pyrite-bearing ores, can be one of the reasons for the low-extracting ability of noble metals.

ACKNOWLEDGMENTS

This work is supported by the Russian Foundation for Basic Research, grant no. 14-05-00504a. The authors thank A.F. Khokhryakov, which gave us a pyrite crystal for research. We thank N.S. Karmanov (Institute of Geology and Mineralogy SB RAS) for the electron microprobe studies of polished sections and V.V. Bakakin (Institute of Inorganic Chemistry SB RAS) for advice. We are sincerely thankful to the associate editor D.I. Foustoukos and anonymous reviewer for their comments and constructive suggestions, which improved this manuscript.

REFERENCES CITED

Abraitis, P.K., Pattrick, R.A.D., and Vaughan, D.J. (2004) Variations in the compositional, textural and electrical properties of natural pyrite: A review. International Journal of Mineral Processing, 74, 41–59.

Arnold, R.G. (1962) Equilibrium relations between pyrrhotite and pyrite from 325° to 741 °C. Economic Geology, 57, 72–90.

Barton, M.D. (1980) The Ag-Au-S system. Economic Geology, 75, 303–316.

Barton, P.B. Jr., and Toulmin, P. (1964) The electrum-tarnish method for the determination of the fugacity of sulfur in laboratory sulfide systems. Geochimica et Cosmochimica Acta, 28, 619–640.

Barton, M.D., Kieft, C., Burke, E.A.J., and Oen, I.S. (1978) Uytenbogaardtite, a new silver–gold sulfide. Canadian Mineralogist, 16 (4), 651–657.

Boyle, R.W. (1968) The geochemistry of silver and its deposits. Geological Survey of Canada, Ottawa, Bulletin 160.

——— (1979) The Geochemistry of Gold and Its Deposits. Geological Survey of Canada, Ottawa, Bulletin 280.

Chareev, D.A., and Osadchii, E.G. (2006) Thermodynamic studies of pyrrhotite–pyrite equilibria in the Ag–Fe–S system by solid-state galvanic cell technique at 518–723 K and total pressure of 1 atm. Geochimica et Cosmochimica Acta, 70, 5617–5633.

Cocker, H.A., Mauk, J.L., and Rabone, S.D.C. (2013) The origin of Ag–Au–S–Se minerals in adularia-sericite epithermal deposits: Constraints from the Broken Hills deposit, Hauraki Goldfield, New Zealand. Mineralium Deposita, 48, 249–266.

Cook, N.J., and Chryssoulis, S.L. (1990) Concentrations of "invisible gold" in the common sulfides. Canadian Mineralogist, 28, 1–16.
Craig, J.R., and Vokes, F.M. (1993) The metamorphism of pyrite and pyritic ores: An overview. Mineralogical Magazine, 57, 3–18.
Fleischer, M. (1955) Minor elements in some sulphide minerals. Economic Geology 50th Anniversary Vol., 970–1024.
Folmer, J.C.W., Hofman, P., and Wiegers, G.A. (1976) Order-disorder transitions in the system $Ag_{2-x}Au_xS$ ($0 < x < 1$). Journal of the Less Common Metals, 48, 251–268.
Francis, D.M. (1971) Electrum-tarnish by sulfur: a study of an irreversible processes. Thesis, Degree Master of Science, The University of British Columbia, 58p.
Gurevich, V.M., Gavrichev, K.S., Tyurin, A.V., Ryumin, M.A., and Osadchii, E.G. (2011) Heat capacity and thermodynamic functions of petrovskaite (AgAuS) at 0–583 K and mineral equilibria in the Ag-Au-S system. Geochemistry International, 49(4), 422–428.
Jin, Z. (1981) A study of the range of stability of phase in some ternary systems. Scandinavian Journal of Metallurgy, 10, 279–287.
Kodentsov, A.A., Bastin, G.F., and Van Loo, F.J.J. (2001) The diffusion couple technique in phase diagram determination. Journal of Alloys and Compounds, 320, 207–217.
Kullerud, G., Yoder, H.S. (1959) Pyrite stability relations in the Fe-S system. Economic Geology, 54, 533–572.
Lambert, J.M., Simkovich, J.R., and Walker, P.L. (1998) The kinetics and mechanism of the pyrite-to-pyrrhotite transformation. Metallurgical and Materials Transactions B, 29B, 385–396.
Osadchii, E.G., and Rappo, O.A. (2004) Determination of standard thermodynamic properties of sulfides in the Ag–Au–S system by means of a solid-state galvanic cell. American Mineralogist, 89, 1405–1410.
Pal'yanova, G.A., Kravtsova, R.G., and Zhuravkova, T.V. (2015b) $Ag_2(S,Se)$ solid solutions in the ores of the Rogovik gold-silver deposit (northeastern Russia). Russian Geology and Geophysics, 56, 1738–1748.
Pal'yanova, G., Mikhlin, Yu., Kokh, K., Karmanov, N., and Seryotkin, Yu. (2015b) Experimental constraints on gold and silver solubility in iron sulfides. Journal of Alloys and Compounds, 649, 67–75.
Palyanova, G.A., Kokh, K.A., and Seryotkin, Yu.V. (2011) Formation of gold and silver sulfides in the system Ag-Au-S. Russian Geology and Geophysics, 52, 443–449.
Palyanova, G.A., Kokh, K.A., and Seryotkin, Yu.V. (2012) Formation of gold-silver sulfides and native gold in Fe-Ag-Au-S system. Russian Geology and Geophysics, 53, 321–329.
Palyanova, G., Karmanov, N., and Savva, N. (2014) Sulfidation of native gold. American Mineralogist, 99, 1095–1103.
Palyanova, G.A., Savva, N.E., Zhuravkova, T.V., and Kolova, E.E. (2016) Gold and silver minerals in low-sulfide ores of the Dzhulietta deposit (northeastern Russia). Russian Geology and Geophysics, 57, 1171–1190.
Proskurnin, V.F., Palyanova, G.A., Karmanov, N.S., Bagaeva, A.A., and Gavrish, A.V. (2011) The first discovery of uytenbogaardtite in Taimyr (Konechnoe occurrence). Doklady Earth Sciences, 441, 1661–1665.
Savva, N.E., Pal'aynova, G.A., and Byankin, M.A. (2012) The problem of genesis of gold and silver sulfides and selenides in the Kupol deposit (Chukotka, Russia). Russian Geology and Geophysics (Geologiya i Geofizika), 53(5), 457–466 (597–609).
Taylor, L.A. (1970) The system Ag-Fe-S: phase equilibria and mineral assemblages. Mineralium Deposita, 5, 41–58.
The Powder Diffraction File PDF-4+ (2006) International Centre for Diffraction Data (ICDD), Release 2006.
Thomas, H.V., Large, R.R., Bull, S.W., Maslennikov, V.V., Berry, R.F., Fraser, R., Froud, S., and Moye, R. (2011) Pyrite and pyrrhotite textures and composition in sediments, laminated quartz veins, and reefs at Bendigo Gold Mine, Australia: Insights for ore genesis. Economic Geology, 106, 1–31.
Tomkins, A.G. (2010) Windows of metamorphic sulfur liberation in the crust: Implications for gold deposit genesis. Geochimica et Cosmochimica Acta, 74, 3246–3259.
Toulmin, P., and Barton, P.B. Jr. (1964) A thermodynamic study of pyrite and pyrrhotite. Geochimica et Cosmochimica Acta, 28, 641–671.
Vaughan, J.P. (2004) The process mineralogy of gold: the classification of ore types. Journal of Metals, 56, 46–48.
Vikentyev, I.V. (2015) Invisible and microscopic gold in pyrite: methods and new data for massive sulfide ores of the Urals. Geology of Ore Deposits, 57, 237–265.
Waldner, P., and Pelton, A.D. (2005) Thermodynamic modeling of the Fe-S system. Journal of Phase Equilibria and Diffusion, 26, 23–38.
Wang, H., and Salveson, I. (2005) A review on the mineral chemistry of the non-stoichiometric iron sulphide, $Fe_{1-x}S$ ($0 \le x \le 0.125$): Polymorphs, phase relations and transitions, electronic and magnetic structures. Phase Transitions, 78, 547–567.
Zhou, J., Jago, B., and Martin, C. (2004) Establishing the process mineralogy of gold ores. SGS Miner. Techical Bulletin, 2004-03, 1–16, http://www.mindat.org/min-4127.html.

Manuscript received April 13, 2016
Manuscript accepted July 25, 2016
Manuscript handled by Dionysis Foustoukos